



Prospects for Observing Astrophysical Transients with Giga-electronvolt Neutrinos

Angelina Partenheimer¹ , Jessie Thwaites¹ , K. Fang¹ , Justin Vandenbroucke¹ , and Brian D. Metzger^{2,3}

¹Department of Physics, Wisconsin IceCube Particle Astrophysics Center, University of Wisconsin, Madison, WI 53706, USA

²Department of Physics, Columbia University, New York, NY 10027, USA

³Center for Computational Astrophysics, Flatiron Institute, 162 5th Avenue, New York, NY 10010, USA

Received 2024 December 12; revised 2025 February 13; accepted 2025 February 15; published 2025 March 21

Abstract

Although Cherenkov detectors of high-energy neutrinos in ice and water are often optimized to detect teraelectronvolt–petaelectronvolt neutrinos, they may also be sensitive to transient neutrino sources in the 1–100 GeV energy range. A wide variety of transient sources have been predicted to emit giga-electronvolt neutrinos. In light of the upcoming IceCube Upgrade, which will extend the IceCube detector’s sensitivity down to a few giga-electronvolts, as well as improve its angular resolution, we survey a variety of transient-source models and compare their predicted neutrino fluences to detector sensitivities, in particular those of IceCube-DeepCore and the IceCube Upgrade. We consider ranges of neutrino fluence from transients powered by nonrelativistic shocks, such as novae, supernovae, fast blue optical transients, and tidal disruption events. We also consider fast radio bursts and relativistic outflows of high- and low-luminosity gamma-ray bursts. Our study sheds light on the prospects of observing giga-electronvolt transients with existing and upcoming neutrino facilities.

Unified Astronomy Thesaurus concepts: [Particle astrophysics \(96\)](#)

1. Introduction

A wide variety of transient sources are predicted to emit giga-electronvolt-energy neutrinos. A growing number of optical transients could be powered entirely or in part by non- or mildly relativistic shocks, which also provide promising sites for proton acceleration and associated hadronic emission (D. Caprioli & A. Spitkovsky 2014; E. Steinberg & B. D. Metzger 2018; K. Fang et al. 2020; A. Bykov et al. 2022). Observational evidence for ion acceleration in shock-powered transients has been accumulated with the recent detections of giga-electronvolt gamma-ray emission from classical (M. Ackermann et al. 2014) and recurrent novae (The Fermi-LAT Collaboration et al. 2010; P. Martin & G. Dubus 2013), the latter also observed to produce teraelectronvolt emission (V. A. Acciari et al. 2022; F. Aharonian et al. 2022). A hadronic interpretation for nova gamma rays is supported by the observed time correlation between the gamma-ray and optical light curves (E. Aydi et al. 2020), the short cooling time of putative gamma-ray-emitting electrons (disfavoring a leptonic origin; e.g., K.-L. Li et al. 2017), and the expected ion versus electron acceleration efficiency at nonrelativistic shocks (D. Caprioli & A. Spitkovsky 2014; R. Xu et al. 2020). Analogous ion acceleration at shocks may occur under similar physical conditions in a wide array of other extragalactic transients (K. Fang et al. 2020), such as interaction-powered supernovae (SNe), tidal disruption events (TDEs), stellar mergers, and fast blue optical transients (FBOTs; N. Roth et al. 2016; T. J. Moriya et al. 2018; R. Margutti et al. 2019).

Besides nonrelativistic transients, relativistic outflows of stellar explosions and outbursts are also promising candidate giga-electronvolt neutrino emitters. Gamma-ray bursts (GRBs), the most powerful explosive events in the Universe, have been

proposed as potential cosmic-ray accelerators (P. Mészáros 2006). Moreover, many models postulate that GRBs could produce high-energy neutrinos without relying on cosmic-ray acceleration; instead, quasi-thermal neutrinos are produced by internal collisions between differentially streaming protons and neutrons as a result of the decoupling of the electrically neutral neutrons (the neutron decoupling scenario; J. N. Bahcall & P. Mészáros 2000) or of the radial differences in the velocities of outflows due to variability in the GRB jet (the collision scenario; A. M. Beloborodov 2010; I. Bartos et al. 2013; K. Murase et al. 2013; A. Zegarelli et al. 2022).

Among GRBs, there exist both high-luminosity (HL) and low-luminosity (LL) varieties, which observations indicate likely comprise two distinct populations of sources (e.g., F. J. Virgili et al. 2009). LLGRBs may similarly produce giga-electronvolt neutrinos following the decoupling model of HLGRBs (K. Murase et al. 2006; N. Gupta & B. Zhang 2007; J. A. Carpio et al. 2024). The GRB population is also divided into long and short (<2 s) classes. While the collisional and decoupling models may be applicable to short GRBs (neutron star mergers), short GRBs are less well understood and may contain other source engines in addition to jets (K. Fang & B. D. Metzger 2017; S. S. Kimura et al. 2017; O. Gottlieb & N. Globus 2021). Therefore, we consider only long GRBs in this work.

Finally, fast radio bursts (FRBs) are millisecond-duration bursts of coherent radio emission (D. R. Lorimer et al. 2007). A promising explanation for FRB observations is based on the flaring activity of magnetars, which can produce neutrino emission due to photohadronic interactions of relativistic ions with surrounding synchrotron photons (B. D. Metzger et al. 2020). The latter occurs in models where FRB emission is produced by magnetized shocks generated as relativistic ejecta from the magnetar flare colliding with some external medium surrounding the FRB site (e.g., B. D. Metzger et al. 2019).

Giga-electronvolt neutrinos help probe the underlying physics of transient sources, as neutrino production is tightly connected to factors such as the composition of the jets, the geometry of



Original content from this work may be used under the terms of the [Creative Commons Attribution 4.0 licence](#). Any further distribution of this work must maintain attribution to the author(s) and the title of the work, journal citation and DOI.

the outflow, and the density of their surrounding media. For example, neutrino production in a GRB is highly inefficient, unless the jet has a significant baryon content. Furthermore, for neutrino production to occur due to neutron decoupling in a GRB, there must be a substantial neutron-to-proton ratio in the GRB jet, which in turn depends on the photodisintegration efficiency at early times (J. N. Bahcall & P. Mészáros 2000) and hence the entropy of the GRB jet (B. D. Metzger et al. 2011; N. Ekanger et al. 2022). Similarly, the internal shock model for GRB neutrino production depends heavily on the proton acceleration efficiency in the GRB (K. Murase et al. 2006). Finally, neutrino production in the magnetar-flaring model of FRBs depends on the upstream medium being composed of baryons (B. D. Metzger et al. 2019, 2020), but this would not be present in alternative scenarios, where the upstream medium is an electron/positron wind (A. M. Beloborodov 2017). In general, the gamma-ray emission from shock-powered transients can arise from either leptonic or hadronic processes, in which case the detection of or constraining limits on gigaelectronvolt neutrino emission would help diagnose the dominant emission mechanisms and the physical conditions at the shock.

The IceCube Neutrino Observatory is a gigaton-scale ice Cherenkov detector located at the geographic South Pole. While the main portion of the detector has sensitivity optimized to the \sim teraelectronvolt–petaelectronvolt range, the center of the detector, called IceCube-DeepCore, contains a more densely instrumented region with sensitivity down to ~ 10 GeV (R. Abbasi et al. 2023a, 2024a). The upcoming IceCube Upgrade, which will add further instrumentation and calibration devices inside the IceCube-DeepCore volume, is expected to improve the sensitivity to $\mathcal{O}(1)$ GeV neutrinos (A. Ishihara 2019). The largest obstacle to gigaelectronvolt neutrino astronomy with IceCube is the neutrino flux generated by cosmic-ray interactions in the atmosphere, which overwhelms the signal from most point sources. However, if the time for which a source is observed is sufficiently small, the signal from a transient source could potentially exceed the threshold necessary for detection before a large amount of atmospheric background has time to accumulate. This makes DeepCore and Upgrade promising for the astronomy of transients emitting gigaelectronvolt neutrinos.

IceCube has conducted extensive searches for gigaelectronvolt neutrinos from various transients, either by looking for emission from an individual event (R. Abbasi et al. 2023b) or by stacking the signals from a population of sources (M. G. Aartsen et al. 2016; R. Abbasi et al. 2022, 2023a, 2023c, 2024a, 2024b). No gigaelectronvolt neutrino transients have been observed to date. Nonetheless, the prospects for gigaelectronvolt transient studies with high-energy neutrinos may still be promising. The IceCube Upgrade and other next-generation facilities will soon provide better sensitivity in the 1–100 GeV range (M. G. Aartsen et al. 2019; P. Kalaczyński 2021). In addition, upcoming optical and infrared observatories, such as the Vera Rubin Observatory and the Nancy Grace Roman Space Telescope, will be able to conduct wider and deeper surveys of the sky, uncovering more transient sources (K. M. Hambleton et al. 2023; I. Andreoni et al. 2024). These surveys could also be complemented by individual bright events, such as a Galactic SN or nova, in the future (S. M. Adams et al. 2013). On the other hand, if further observations at increasing sensitivity continue to yield

nondetections of gigaelectronvolt neutrinos from transient sources, this would establish strong constraints on our understanding of the composition and environment of transient sources. Because of this, continued observation of transient sources with improved sensitivity at 1–100 GeV will have fundamental implications for our understanding of many types of astrophysical sources.

In this paper, we survey models of neutrino emission from a number of transient-source classes to estimate their predicted neutrino fluence (time-integrated energy flux) and timescale suitable for observation. We compare these results to the sensitivity of IceCube-DeepCore and the projected sensitivity of IceCube Upgrade. In Section 2, we outline the models used for our fluence estimates. In Section 3, we estimate the sensitivities of Upgrade and DeepCore as a function of observation time, and in Section 4, we present our results.

2. Transient Models

2.1. Shock-powered Transients

We base our fluence estimate for shock-powered transients on K. Fang et al. (2020), which extends observations of classical novae to be applicable to nonrelativistic shocks in SNe, novae, TDEs, and FBOTs. In this model, each transient is modeled as uniform, spherically expanding ejecta colliding with a stationary external medium. This collision creates a shock moving forward into the stationary medium and a reverse shock traveling back into the ejecta. The shock observables are the optical luminosity curve L_{opt} , the peak time t_{pk} , and the mean velocity of the shocked ejecta v_{ej} .

During the initial phases of the shock’s outward propagation, the external medium is too opaque for radiation to escape the environment. Instead, thermal emission (e.g., UV or X-ray photons) from the shocked gas is absorbed by the ejecta and efficiently reprocessed to optical light. When the optical depth of the material ahead of the expanding shock has dropped below the critical value $\tau_{\text{opt}} \approx c/v_{\text{sh}}$, this reprocessed optical radiation can escape the shock, to a distant observer. This transition occurs at the critical time t_{pk} , which coincides with the peak of the transient’s optical light curve. Because of this, after time t_{pk} , the kinetic power of the shock should faithfully track the observed optical luminosity: $L_{\text{sh}} \approx L_{\text{opt}}$. We thus make the optimistic assumption that all of the transient’s light is powered by reprocessed shock emission, with only small contributions from other sources of luminosity potentially present in these sources, such as radioactivity or a central compact object.

Not only is the optical emission that escapes from the shock suppressed at times earlier than t_{pk} , but relativistic ion acceleration is also difficult, because the shock transition is mediated by radiation instead of being collisionless during these phases (see A. Levinson & E. Nakar 2020 for a review of radiation-mediated shocks). Instead, the bulk of the particle acceleration must occur after t_{pk} . The accelerated ions during this latter phase carry power $\dot{L}_{\text{rel}} \approx \epsilon_{\text{rel}} L_{\text{sh}}$, where ϵ_{rel} is the particle acceleration efficiency. In classical novae, this efficiency is measured to be $\epsilon_{\text{rel}} \sim 0.003$ – 0.01 (B. D. Metzger et al. 2015; E. Aydi et al. 2020), based on the observed ratio of gamma-ray to optical luminosities (the gamma-ray luminosity tracks the fraction of the shock power into nonthermal particles, while the optical luminosity tracks the total shock power); in our fluence estimates, we consider a range of efficiencies

$\epsilon_{\text{rel}} = 0.01\text{--}0.1$, which bracket the measured values in novae and the $\sim 10\%$ maximum ion acceleration efficiency predicted for nonrelativistic shocks by particle-in-cell simulations (D. Caprioli & A. Spitkovsky 2014).

We assume that the protons accelerated at the shock follow a standard power-law energy spectrum $\frac{dN}{dE_p} \propto E_p^{-\alpha}$, where α is the spectral index (e.g., E. Steinberg & B. D. Metzger 2018). We consider a range of values $\alpha = 2\text{--}2.7$. The proton spectrum is normalized by the total energy output over the transient’s duration Δt , viz:

$$\int dE_p E_p \frac{dN}{dE_p} = \int_{t_{\text{pk}}}^{t_{\text{pk}} + \Delta t} L_{\text{rel}} dt. \quad (1)$$

We estimate Δt as the time from the peak luminosity t_{pk} to when the shock power/neutrino luminosity has dropped to half its peak value. For the transient classes we consider, this timescale ranges from a few days for novae to a few months for TDEs.

After leaving the vicinity of the shock, the accelerated protons collide with other ambient ions, generating pions that subsequently decay into neutrinos and gamma rays. The neutrino $E^2 dN/dE dA$ from a nearby (i.e., noncosmological) source at distance d_{min} can be estimated by

$$E_\nu^2 \frac{dN}{dE_\nu dA} = \frac{1}{2} E_p^2 \frac{dN}{dE_p} f_{\text{pp}} \frac{1}{4\pi d_{\text{min}}^2}, \quad (2)$$

where the factor of $1/2$ arises because charged pions are produced with a probability of two-thirds in proton–proton interactions and about three-quarters of the charged pion energy is carried away by neutrinos. Here, $f_{\text{pp}} = 1 - \exp(-t_{\text{dyn}}/t_{\text{pp}}) = 1 - \exp(-\tau_{\text{pp}} c/v_{\text{sh}})$ is the pion production efficiency, and $\tau_{\text{pp}} \approx n_{\text{sh}} \sigma_{\text{pp}} R_{\text{sh}}$ is the optical depth to proton–proton production, where σ_{pp} is the inelastic proton–proton cross section. Following the discussion above, we normalize n_{sh} , such that the peak emission timescale t_{pk} equals the critical “Arnett” timescale, at which the photon diffusion time through the ejecta external to the shock and the adiabatic loss time are equal (W. D. Arnett 1982). After the peak $t > t_{\text{pk}}$, the radial profile of n_{sh} encountered by the shock is chosen such that the kinetic luminosity of the shock matches the transient’s optical light curve, under the assumption of a constant radial shock speed.

We evaluate the spectra of secondary neutrinos using `Aafragpy` (S. Koldobskiy et al. 2021). In particular, we use the model from M. Kachelrieß et al. (2019) to evaluate the pp cross section above 4 GeV, and we use the model from T. Kamae et al. (2006) for the cross section below 4 GeV.

We divide the shock-powered transients into five broad source classes: novae, luminous red novae (LRNe), SNe, TDEs, and FBOTs. For each case, we employ a light-curve “template” normalized to the peak luminosity L_{pk} and timescale t_{pk} of each transient subtype. The adopted ranges of volumetric rates, peak luminosity, and ejecta velocity for each follow those compiled in Table 1 of K. Fang et al. (2020), while t_{peak} is taken as the mean of the given range.

Novae. A number of novae have been detected over the past ~ 15 yr in gigaelectronvolt–teraelectronvolt gamma rays. These include over a dozen classical novae (The Fermi-LAT Collaboration 2014; C. C. Cheung et al. 2016; K.-L. Li et al. 2017; E. Aydi et al. 2020) as well as a few recurrent novae

(P. Martin & G. Dubus 2013), most recently RS Ophiuchi (V. A. Acciari et al. 2022; F. Aharonian et al. 2022; C. C. Cheung et al. 2022). For classical novae, we use a light-curve template of a nova eruption on a solar-mass white dwarf from I. Hachisu & M. Kato (2018). We use the volumetric rates from A. W. Shafter (2017) and C. S. Kochanek (2014), considering separately events in our Galaxy versus extragalactic novae. For Galactic rates, we approximate the Galaxy as a thin disk of radius 20 kpc centered about the Sun. Based on the Galactic nova rate of $27\text{--}81 \text{ yr}^{-1}$ from A. W. Shafter (2017), we infer an event surface density $\Sigma_{0,\text{GN}}$, from which we estimate the distance to the nearest Galactic event $d_{\text{min}} = (\pi t_{\text{obs}} \Sigma_{0,\text{GN}})^{-1/2}$ Gpc, over a given observing duration t_{obs} .

We note that the teraelectronvolt gamma-ray emission in recurrent novae such as RS Oph (V. A. Acciari et al. 2022; F. Aharonian et al. 2022; C. C. Cheung et al. 2022) may originate from distinct shocks, located at larger distances from the white dwarf than the more compact shocks that produce the gigaelectronvolt emission (R. Diesing et al. 2023). Because of the lower density of the shocked gas in this case, the optical light curve may no longer directly trace the shock power contributing to the teraelectronvolt emission. For this reason, and because the focus of this work is on gigaelectronvolt emission, we omit this emission component from our modeling.

LRNe. Similar to classical novae, LRNe from stellar mergers are likely at least in part powered by shock interaction (B. D. Metzger & O. Pejcha 2017; T. Matsumoto & B. D. Metzger 2022). For this source class, we adopt the light curve of V1309 Sco as the template (E. Mason et al. 2010; R. Tytenda et al. 2011; T. Matsumoto & B. D. Metzger 2022) and a volumetric rate of 0.2 yr^{-1} per Galaxy from G. Howitt et al. (2020). V1309 Sco was a Galactic LRN with a firm association with merging binary stars. It is one of the dimmest but volumetrically most common types of LRNe.

SNe. To date, nonthermal gamma-ray emission has not been observed from SNe (M. Ackermann et al. 2015; N. Renault-Tinacci et al. 2018). It has been suggested that a dense circumstellar medium around SNe could attenuate the teraelectronvolt gamma-ray signal, which would conceal the signatures of internal shocks (J. E. Andrews & N. Smith 2018; P. Cristofari et al. 2020). Because of this, SNe are still anticipated to be significant sources of high-energy neutrinos (K. Murase et al. 2019). We consider all core-collapse SNe (CCSNe) as a subset, and we additionally consider the class of SNe IIn only, which are a subset of CCSNe with clear evidence for shock interaction. The CCSN rate is obtained from M. Taylor et al. (2014), and the rate of SNe IIn is taken to be 8.8% of the CCSNe, following W. Li et al. (2011). We also evaluate the fluence of both Type I and Type II superluminous SNe (SLSNe), which are SNe with very high optical luminosity (T. J. Moriya et al. 2018). The SLSN rates are obtained from R. M. Quimby et al. (2013). Finally, a small subset of Type Ia SNe with evidence for shock interaction between the ejecta and circumstellar material (Type Ia CSM) show evidence for shock powering (C. D. Bochenek et al. 2017), and we estimate their fluence assuming they represent 0.1%–1% of the SN Ia rate (B. Dilday et al. 2012). For our SN light-curve template, we use the light curve of a typical SLSNe II from C. Inserra (2019).

TDEs. TDEs are optical and UV transients (S. Gezari et al. 2012; I. Arcavi et al. 2014; N. C. Stone & B. D. Metzger 2015)

whose light curves may be powered by shocks (T. Piran et al. 2015; Y.-F. Jiang et al. 2016). TDEs are predicted to be emitters of high-energy neutrinos and gamma rays (L. Dai & K. Fang 2017; C. Guépin et al. 2018; K. Murase et al. 2020; W. Winter & C. Lunardini 2023). We use the light-curve template of the TDE event PTF09ge from S. van Velzen et al. (2020). The rate of TDEs is consistent with N. C. Stone & B. D. Metzger (2015) and S. v. Velzen (2018); the range of peak luminosities is obtained from S. v. Velzen (2018), and the peak time is obtained from B. Mockler et al. (2019).

FBOTs. FBOTs are fast, luminous, UV-bright transients that exhibit characteristics similar to SNe, but have timescales and luminosities inconsistent with traditional SN models (M. R. Drout et al. 2014; D. L. Coppejans et al. 2020). The class of sources producing FBOTs is unknown, and some models postulate shock powering as an explanation for their observed characteristics (R. Margutti et al. 2019). High-energy neutrinos from FBOTs have been studied in K. Fang et al. (2019). The nearby event AT2018cow provides a particularly well-studied case of such a transient (D. A. Perley et al. 2018), and we use its light curve as our template. The rates and peak times of FBOTs are derived from M. R. Drout et al. (2014). We consider separately the category of especially luminous FBOTs ($M_g < -19$), of which AT2018cow is an example. For luminous FBOTs, the rate is taken from D. L. Coppejans et al. (2020) and the peak time is based on S. J. Prentice et al. (2018).

2.2. GRBs

In this section, we estimate the expected fluence of HL and LL GRBs. We consider both decoupling and collisional scenarios for the HLGRB and the decoupling scenario for the LLGRB. We obtain the total expected fluence for each case following K. Murase et al. (2022), who apply the decoupling and collisional models to the recent event GRB 221009A; we reiterate their fluence calculation below. The parameters that we input to our GRB models are the bulk Lorentz factor Γ and the isotropic-equivalent gamma-ray energy $\mathcal{E}_{\gamma, \text{iso}}$, as well as GRB rates.

In the neutron decoupling scenario, the neutron and proton populations in the GRB jet are initially coupled by nuclear elastic scattering. As the bulk np outflow expands, the scattering time eventually exceeds the comoving expansion time, at which point the neutron population decouples from the proton population. If the decoupling occurs while the outflow is still accelerating (before $\Gamma = \Gamma_{\text{max}}$), the proton flow continues to be accelerated by proton coupling to photons, while the neutron flow begins to coast. In this way, the neutron and proton flows can acquire a drift velocity, causing inelastic np collisions.

The energy of neutrinos produced in the decoupling process is given by

$$E_\nu \approx 0.1\Gamma_{n,\text{dec}}m_p c^2 / (1+z). \quad (3)$$

Here, $\Gamma_{n,\text{dec}}$ is the Lorentz factor of neutrons at decoupling, and it is estimated to be

$$\Gamma_{n,\text{dec}} = \frac{3}{4} \left(\frac{L_p \sigma_{np} \Gamma_*}{4\pi R_* \Gamma_{\text{max}} m_p c^3} \right)^{1/3}, \quad (4)$$

where $\Gamma_* = 10$ and $R_* = 10^{11}$ cm are the breakout Lorentz factor and injection radius, which have been set to fiducial values, and $\sigma_{np} \approx 3 \times 10^{-26}$ cm² is the neutron–proton cross

section. The proton luminosity L_p is evaluated as $L_p \sim \xi_N \mathcal{E}_\gamma^{\text{iso}} / \Delta t$. We use a range of nucleon loading factors $\xi_N = 3\text{--}30$, as suggested by K. Murase et al. (2022), and we account for this range of loading factors in the uncertainty of our final fluence calculation. The total flavor-summed ($\nu + \bar{\nu}$) neutrino fluence is estimated as

$$\int dE_\nu E_\nu \frac{dN}{dE_\nu dA} \approx \frac{1}{4} \frac{(1+z)}{4\pi d_L^2} \zeta_n \left(\frac{\Gamma_{n,\text{dec}}}{\Gamma} \right) \xi_N \mathcal{E}_\gamma^{\text{iso}}, \quad (5)$$

where we assume that the number ratio of protons to neutrons is $\zeta_n = 1$. In np collisions, two-thirds of the produced pions are charged, and three-quarters of their decay products are shared by each flavor of neutrinos. Additionally, the nucleon inelasticity of np collisions is ≈ 0.5 , altogether contributing the factor of $1/4$.

Because the GRB jet itself is variable, neutrons from a slower region may also diffuse into a faster region of the jet, creating a compound flow with $\Gamma_n < \Gamma_p$, resulting in neutrino production from inelastic np collisions. These collisions can occur even in cases where the np decoupling occurs after $\Gamma = \Gamma_{\text{max}}$ is achieved, and the relative velocities between the proton and neutron flows are not sufficient to produce pions in np collisions from decoupling alone.

The expected energy of the neutrinos produced in the collisional process is

$$E_\nu \approx 0.1\Gamma'_{\text{rel}} m_p c^2 / (1+z), \quad (6)$$

giving 30–300 GeV neutrinos. Here, $\Gamma'_{\text{rel}} \sim 2$ is the relative Lorentz factor of the interacting flow. The flavor-summed ($\nu + \bar{\nu}$) neutrino fluence is given by

$$\int dE_\nu E_\nu \frac{dN}{dE_\nu dA} \approx \frac{1}{4} \frac{(1+z)}{4\pi d_L^2} \xi_N \tau_{pn} \mathcal{E}_\gamma^{\text{iso}}, \quad (7)$$

where we assume the pn optical depth is $\tau_{pn} = 1$.

As in the case of shock-powered transients, we evaluate the spectra of GRB neutrinos using `Aafragpy` (T. Kamae et al. 2006; M. Kachelrieß et al. 2019; S. Koldobskiy et al. 2021). For the decoupling scenario, we evaluate the neutrino spectra from a monoenergetic spectrum of rest-mass energy protons. In the collisional scenario, where a wider range of proton energies can contribute to neutrino production, we use a primary proton spectrum following a Maxwell–Boltzmann distribution with a mean energy of the proton rest mass

$$\frac{dN}{dE_p} \propto 2\sqrt{\frac{E_p}{\pi}} \left(\frac{1}{kT} \right)^{3/2} e^{-E_p/kT} \quad (8)$$

with $kT = \frac{2}{3}m_p c^2$.

The spectra are normalized such that the total fluence is equivalent to the values given by Equations (5) and (7). We normalize the spectral peaks so that the peak energy aligns with the values predicted by Equations (3) and (6). We outline the parameters used for HL and LL GRBs below.

HLGRBs. For HLGRBs, we consider neutrino production both in the decoupling and collisional scenarios. We consider the ranges $\Gamma = 100\text{--}1000$ and $E_{\gamma, \text{iso}} = 10^{52}\text{--}10^{54}$ erg (J.-L. Atteia et al. 2017; J. N. Bahcall & P. Mészáros 2000; K. Murase et al. 2022), as well as an observational time window $\Delta t = 100$ s, based on the T90 values presented in J.-L. Atteia et al. (2017). We use a range of true GRB rates $R_{0,\text{HL}} = 0.5\text{--}2$ Gpc⁻³ yr⁻¹ (D. Wanderman & T. Piran 2010),

which give a conservative estimate of the nearest HLGRB that may produce neutrinos detectable at Earth.

LLGRBs. LLGRBs likely comprise a distinct population of sources from their HL counterparts. However, the decoupling model from HLGRBs is often considered when modeling LLGRBs. For LLGRBs, we use $\Gamma = 10\text{--}100$ and $E_{\gamma,\text{iso}} = 10^{49}\text{--}10^{51}$ erg (K. Murase et al. 2006; J. A. Carpio et al. 2024) and an observational time window $\Delta t = 20$ s (T. Piran 2005; E. Nakar 2015). We use a range of geometrically corrected LLGRB rates of $R_{0,\text{LL}} = 200\text{--}500$ Gpc $^{-3}$ yr $^{-1}$, following K. Murase et al. (2006).

2.3. FRBs

We base our FRB fluence estimates on B. D. Metzger et al. (2020), who calculate the neutrino emission from a shock generated by ejecta from a magnetar flare colliding with an external baryon-loaded medium (e.g., an earlier ejecta shell from the same magnetar; B. D. Metzger et al. 2019). The model is motivated in part by observations of the Galactic FRB 200428, which was observed in coincidence with an X-ray outburst from the Galactic magnetar SGR 1935+2154 (C. D. Bochenek et al. 2020). To date, this is the only FRB observed from our Galaxy with properties broadly consistent with those of extragalactic FRBs (typically at cosmological distances), and its fluence was still at the very low end of this range. Nevertheless, we focus in this paper on the detection prospects for a Galactic FRB but with properties more energetic and hence typical of the cosmological FRB population than FRB 200428.

We consider only neutrino production from the thermal population of ions heated at the relativistic shock (as opposed to neutrinos from the nonthermal ions accelerated by the shock, which generate higher-energy \gtrsim teraelectronvolt neutrinos; B. D. Metzger et al. 2020). In the following discussion, the primed frame refers to the comoving frame of the relativistic outflow. The FRB observables are its duration t_{FRB} , radio frequency ν_{obs} , and radio energy $\mathcal{E}_{\text{radio}}$. These can be related to the shock radius r_{FRB} , density n_{FRB} , Lorentz factor of the shock Γ_{FRB} , and luminosity of the FRB L_{FRB} through Equations (5)–(10) of B. D. Metzger et al. (2020).

In the case of a uniform density profile of the external medium, the shock parameters evolve with time as

$$\begin{aligned}\Gamma &= \Gamma_{\text{FRB}} \left(\frac{t}{t_{\text{FRB}}} \right)^{-3/8} \\ r_{\text{sh}} &= r_{\text{FRB}} \left(\frac{t}{t_{\text{FRB}}} \right)^{1/4} \\ L_{\text{sh}} &= L_{\text{FRB}} \left(\frac{t}{t_{\text{FRB}}} \right)^{-1}.\end{aligned}$$

We assume that the shock's energy is shared equally between protons and electrons in the plasma, where both are heated to Maxwellian energy distributions (L. Sironi & A. Spitkovsky 2010). The heated electrons emit synchrotron radiation, which peaks at the photon energy

$$\epsilon_{\text{pk}} = \frac{\hbar e B'}{m_e c} \bar{\gamma}^2 \Gamma, \quad (9)$$

which is on the order of hundreds of megaelectronvolts. Here, $B' = \sqrt{64\pi\sigma\Gamma^2 m_p c^2 n_{\text{FRB}}}$ is the post-shock magnetic field and $\bar{\gamma} = (m_p/m_e)\Gamma/2$ is the mean thermal Lorentz factor.

We consider neutrino production from a distribution of thermal protons with mean energy $E'_p = \Gamma m_p c^2/2$ immersed in a field of monoenergetic photons at energy $\epsilon'_\gamma = \epsilon_{\text{pk}}/\Gamma$. The energy of the protons that interact with the synchrotron photons is evaluated as $E'_p = E'_\Delta m_p c^2 / (2\epsilon'_\gamma)$, where $E'_\Delta \approx 0.3$ GeV is the Δ -resonance energy. The pion production by thermal protons lasts until ϵ'_γ and then drops so much that the threshold condition is no longer satisfied for mean-energy thermal protons. Beyond that time, pion production can only occur to nonthermal protons. We use this time t_{nth} as the value for Δt over which the FRB is observed. This timescale, which is much shorter than for any other transient source, falls into a fully background-free regime for IceCube observation.

The proton energy spectrum follows a relativistic Maxwell–Boltzmann distribution:

$$\frac{dN}{dE_p} \propto \frac{dN}{d\gamma_p} = \frac{\left(\frac{\gamma_p}{\Gamma}\right)^2 e^{-\gamma_p/\Gamma\Theta}}{2\Gamma\Theta^3}, \quad (10)$$

where $\gamma_p = E_p/m_p c^2$ and $\Theta = \frac{1}{3}(\Gamma/2)$. The distribution is normalized to reflect the total shock energy conferred to protons during the thermal period, or $\frac{1}{2} \int^{t_{\text{nth}}} L_{\text{sh}} dt$. The neutrino $E'_\nu dN/dE'_\nu dA$ from an FRB at distance d is estimated by

$$E'_\nu \frac{dN}{dE'_\nu dA} = \frac{1}{4\pi d^2} \frac{3}{8} \tau_{p\gamma} E_p^2 \frac{dN}{dE_p}, \quad (11)$$

where the factor of $3/8$ accounts for the fraction of proton energy that goes into neutrinos during a $p\gamma$ interaction. The optical depth of the $p\gamma$ interaction is given by $\tau_{p\gamma} \approx n'_\gamma \sigma_{p\gamma} r'$, where $\sigma_{p\gamma}$ is the inelastic $p\gamma$ interaction cross section, and $n'_\gamma \approx u'_\gamma/\epsilon'_{\text{pk}}$ and $r' \approx r_{\text{sh}}/\Gamma$ are the photon number density and radius of the post-shock region in the comoving frame, respectively. The radiated power is estimated as $u'_\gamma \approx (\frac{1}{2}L_{\text{sh}})/(4\pi r_{\text{sh}}^2 c\Gamma^2)$, considering that about half of the shock power goes to thermal electrons. Note that in a typical FRB, the thermal proton energy is too high for Bethe–Heitler pair production to be significant. The energy of a synchrotron photon in the rest frame of a thermal proton is on the order of hundreds of megaelectronvolts, where the effective cross section (the product of the cross section and inelasticity) is very suppressed.

For our estimate, we use $\mathcal{E}_{\text{radio}} = 10^{37}\text{--}10^{41}$ erg and $t_{\text{FRB}} = 0.1\text{--}10$ ms, which are typical for most extragalactic FRBs. We use an optimistic distance $d = 10$ kpc, which is the distance of Galactic FRB 200428. FRB 200428 was the only observed Galactic FRB with parameters comparable to the extragalactic FRB population, and the Galactic FRB rate is poorly constrained. The event FRB 200428 had a radio energy of 10^{35} erg, so our estimate is quite optimistic and depends on a more typical FRB occurring in our Galaxy during the next decade.

3. Estimation of IceCube Sensitivity

In this section, we estimate the sensitivities of IceCube Upgrade and DeepCore as a function of observation time. Our

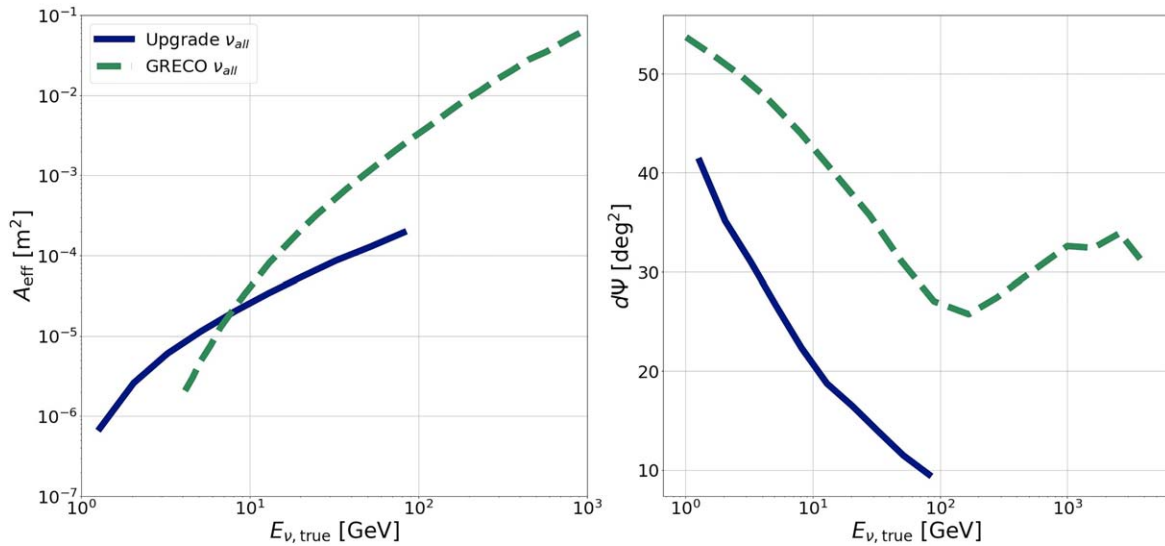


Figure 1. Flavor-summed ($\nu + \bar{\nu}$) effective area and angular resolution of GRECO and Upgrade. The GRECO data set is optimized for 10 GeV–1 TeV; Upgrade is intended to provide additional sensitivity to events at 1–10 GeV. We obtain the GRECO northern sky effective area and median angular resolution from R. Abbasi et al. (2024a). We evaluate the expected Upgrade parameters using simulated data provided by IceCube Collaboration (2020). The effective area for GRECO is averaged over the northern sky, while the effective area for Upgrade is averaged over the full sky.

approach to estimating the sensitivity is an analytic approximation that is intended to give perspective on the potential detection prospects for various transient types and should not be considered as a formal evaluation of IceCube’s sensitivity. In particular, a formal estimation of IceCube’s sensitivity would use a log-likelihood method over the full energy range of the data set. In addition, such an estimate would consider event-by-event angular resolution rather than the median angular resolution, and it would evaluate the sensitivity for a source at a specific decl., while our estimate considers an average sensitivity over a broad range (averaged over the northern hemisphere for the GeV Reconstructed Events with Containment for Oscillation or GRECO sample and all-sky-averaged for Upgrade). Such targeted searches may improve the sensitivity over the estimates shown here. Nevertheless, our analytic estimate is a reasonable proxy of the IceCube sensitivity for the broad orders-of-magnitude comparisons we make in this analysis. Our method for estimating the sensitivities of IceCube-DeepCore and the IceCube Upgrade are outlined below.

We obtain atmospheric neutrino flux estimates from M. Honda et al. (2015). We evaluate the total flavor-summed number of observed atmospheric neutrinos using

$$N_{\text{atm}} = t_{\text{obs}} \int_{E_{\text{min}}}^{E_{\text{max}}} \frac{dN}{dEdAd\Omega dt} A_{\text{eff}} \Omega dE,$$

where E_{min} , E_{max} give the energy range of the observation, A_{eff} is the effective area of the detector, t_{obs} is the observation time, and $\Omega = d\Psi^2$ is the solid angle of the detector’s resolution, which is evaluated using a median angular resolution $d\Psi$. For sufficiently low observation times, there may be no observed background events; the time interval over which this condition is met is considered the “background-free” regime.

Our estimate of the sensitivity follows the formalism for the case of a Poisson distribution with known background, as described in V. L. Kashyap et al. (2010), which we briefly outline here. For an observation over a given time interval t_{obs} , we constrain the probability of a false-positive detection α

using

$$\Pr(N_s > N_s^* | \lambda_s = 0, \lambda_{\text{atm}}, t_{\text{obs}}) = \frac{\gamma(N_s^* + 1, N_{\text{atm}})}{\Gamma(N_s^* + 1)} \leq \alpha,$$

where $\alpha = 0.1$, $N_{\text{atm}} = \lambda_{\text{atm}} t_{\text{obs}}$, and N_s^* gives the number of events at the threshold. Here, $\gamma(a, x)$ is the incomplete gamma function, as defined in Equation (8.350.1) of I. Gradshteyn & I. Ryzhik (2007). We constrain the probability of detection at the threshold β using

$$\Pr(N_s > N_s^* | \lambda_s, \lambda_{\text{atm}}, t_{\text{obs}}) = \frac{\gamma(N_s^* + 1, N_s^* + N_{\text{atm}})}{\Gamma(N_s^* + 1)} = \beta,$$

taking $\beta = 0.9$. This yields the number of signal events $N_{s,90}$ necessary for a source to exceed the background-only expectation over a given observation time t_{obs} .

We assume a source power-law spectrum $dN/dE \propto E^{-s}$, where s is the source spectral index. This gives an expected number of observed signal neutrinos:

$$N_s = K \int_{E_{\text{min}}}^{E_{\text{max}}} E^{-s} A_{\text{eff}} dE,$$

where the coefficient K is a normalization factor. Taking $K = N_{s,90}/N_s$ gives the spectrum at the detection threshold. The minimum fluence (time-integrated energy flux) necessary for a neutrino source to be detected over the atmospheric background is then

$$F_{\nu,\text{lim}} = K \int_{E_{\text{min}}}^{E_{\text{max}}} E^{(1-s)} dE.$$

For both GRECO and Upgrade, we consider the effective area for all neutrino flavors ($\nu + \bar{\nu}$). To estimate the sensitivity of IceCube-DeepCore, we use the GRECO (GeV Reconstructed Events with Containment for Oscillation) data set. This data set is optimized for observations at 10 GeV–1 TeV and is often used to search for low-energy transients. In the case of GRECO, we use an effective area averaged over the northern sky (which gives a slightly more optimistic sensitivity estimate

Table 1
Ranges of Values Used to Evaluate the Estimates of Figure 3

Source	\mathcal{R}_0 ($\text{Gpc}^{-3} \text{ yr}^{-1}$)	$\log_{10} L_{\text{pk}}$ (erg s^{-1})	t_{pk} (days)	\bar{v}_{ej} (10^3 km s^{-1})
Novae	$(1-5) \times 10^8$	37–39	3	0.5–3
LRNe	$10^{5.5-10^{6.4}}$	38–41	100	0.2 - 0.5
SLSNe I	10–100	43.3–44.5	40	5–10
SLSNe II	70–300	43.6–44.5	33.5	5–10
SNe IIn	3000	42–43.7	35	5
CCSNe	$7-10^4$	41.9–42.9	13.5	3
Type Ia CSM	300–3000	~ 43	20	10
TDE	100–1000	44–45	120	5–15
FBOT	$\sim 4800-8000$	~ 43	8	6–30
Lum. FBOT	$\sim 700-1400$	~ 44	3	6–30
Galactic novae	$27-81 \text{ yr}^{-1}$	37–39	3	0.5–3
Galactic LRNe	0.2 yr^{-1}	38–41	100	0.2–0.5
Galactic CCSNe	10 kpc	41.9–42.9	13.5	3
GRB	\mathcal{R}_0 ($\text{Gpc}^{-3} \text{ yr}^{-1}$)	Γ	$\mathcal{E}_{\gamma, \text{iso}}$ (erg)	ξ_N
HL	0.5–2	100–1000	$10^{52}-10^{54}$	3–30
LL	200–500	10–100	$10^{49}-10^{51}$	3–30
	d (kpc)	t_{FRB} (ms)	$\mathcal{E}_{\text{radio}}$ (erg)	
FRB	10	0.1–10	$10^{37}-10^{41}$	

Note. The ranges of values are chosen to encompass the broad range of parameters expected for each transient type. In the case of shock-powered transients, we use the observational values summarized in K. Fang et al. (2020); we also use a range of spectral indices $\alpha = 2-2.7$ and a particle acceleration efficiency $\epsilon_{\text{rel}} = 0.01-0.1$. For the FRB model, we use the typical FRB ranges derived by B. Margalit et al. (2020), and we use the distance of the Galactic event FRB 200428. For GRBs, we use ranges of the bulk Lorentz factor Γ and isotropic-equivalent gamma-ray energy $\mathcal{E}_{\gamma, \text{iso}}$, consistent with the ranges cited by J.-L. Atteia et al. (2017), K. Murase et al. (2022), and J. N. Bahcall & P. Mészáros (2000) for HL and by K. Murase et al. (2006) and J. A. Carpio et al. (2024) for LL. We use the ranges of GRB rates estimated by K. Murase et al. (2006) and D. Wanderman & T. Piran (2010) and the range of particle acceleration efficiencies presented by K. Murase et al. (2022).

than the southern sky). We obtain the GRECO effective area and angular spread of events $\Delta\Psi$ from R. Abbasi et al. (2024a); we multiply the effective area presented in R. Abbasi et al. (2024a) by 2 to give a flavor-summed ($\nu + \bar{\nu}$) estimate, and we use the median value of $\Delta\Psi$.

The upcoming IceCube Upgrade, which will add further instrumentation and calibration devices to IceCube-DeepCore, is expected to improve the sensitivity to $\mathcal{O}(1 \text{ GeV})$ neutrinos. We obtain a projection of the effective area and angular resolution of Upgrade using simulated IceCube Upgrade detector data provided by IceCube Collaboration (2020). For the case of IceCube Upgrade, we consider the effective area averaged over the whole sky. It should be noted that the estimates of the effective area and angular resolution presented in

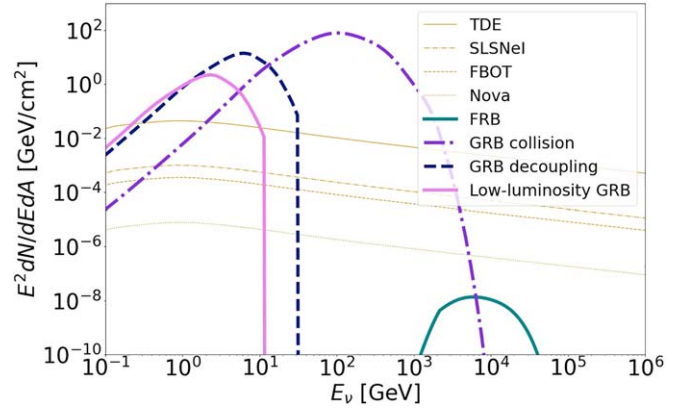


Figure 2. $E^2 dN/dEdA$ of various transient sources. The spectra of four shock-powered transient-source types are shown with spectral index $\alpha = 2.4$ and are normalized to the mean values shown in Table 1. The FRB spectrum for thermal neutrino emission is evaluated using the fiducial parameters $t_{\text{FRB}} = 1 \text{ ms}$ and $\mathcal{E}_{\text{radio}} = 10^{40} \text{ erg}$, with $d = 10 \text{ kpc}$. In the case of an HLGRB, the spectra are shown separately for the decoupling and collision models; in the case of an LLGRB, the spectrum is shown for the decoupling model only. All GRB spectra are normalized using mean values from Table 1.

IceCube Collaboration (2020) should be considered preliminary, and these values may be further optimized in the future. We show the effective area and angular resolutions of GRECO and Upgrade in Figure 1. We evaluate the sensitivities assuming source spectral indices ranging from $s = 1.5$ to $s = 3$.

4. Results

The ranges of the parameters used in our fluence predictions for various transient classes are summarized in Table 1. For extragalactic events, we estimate the nearest event within t_{obs} years of the IceCube observation using the event’s volumetric birth rate $R_0 \text{ Gpc}^{-3} \text{ yr}^{-1}$:

$$d_{\text{min}} \sim \left(\frac{4\pi}{3} t_{\text{obs}} R_0 \right)^{-1/3} \text{ Gpc}. \quad (12)$$

Figure 2 shows time-integrated, energy-scaled spectra ($E^2 dN/dEdA$) of several transients considered in this work. The spectra shown use mean values from Table 1. For shock-powered transients, the spectral index $\alpha = 2.4$ is shown, although in our fluence estimate, we consider the range of values $\alpha = 2-2.7$. The expected fluence of a transient over a particular energy interval is given by integrating its (already time-integrated) energy spectrum over the desired energy interval:

$$F_\nu = \int_{E_{\text{min}}}^{E_{\text{max}}} dE_\nu E_\nu \frac{dN}{dE_\nu dA}. \quad (13)$$

For perspective, we also show an optimistic estimate of a Galactic CCSN at 10 kpc. The true rate of Galactic CCSNe is \sim three per century (S. M. Adams et al. 2013), so there is only a $\sim 30\%$ chance of such an event occurring in the Galaxy in the next decade. However, if such an event were to occur, the prospects for detection could be favorable.

The expected neutrino fluence (time-integrated energy flux) of the nearest transients in 10 yr of observations is shown in Figure 3. The fluence estimates are evaluated using the mean values from the ranges in Table 1. We compare these to the IceCube sensitivity, also integrated over the same energy range

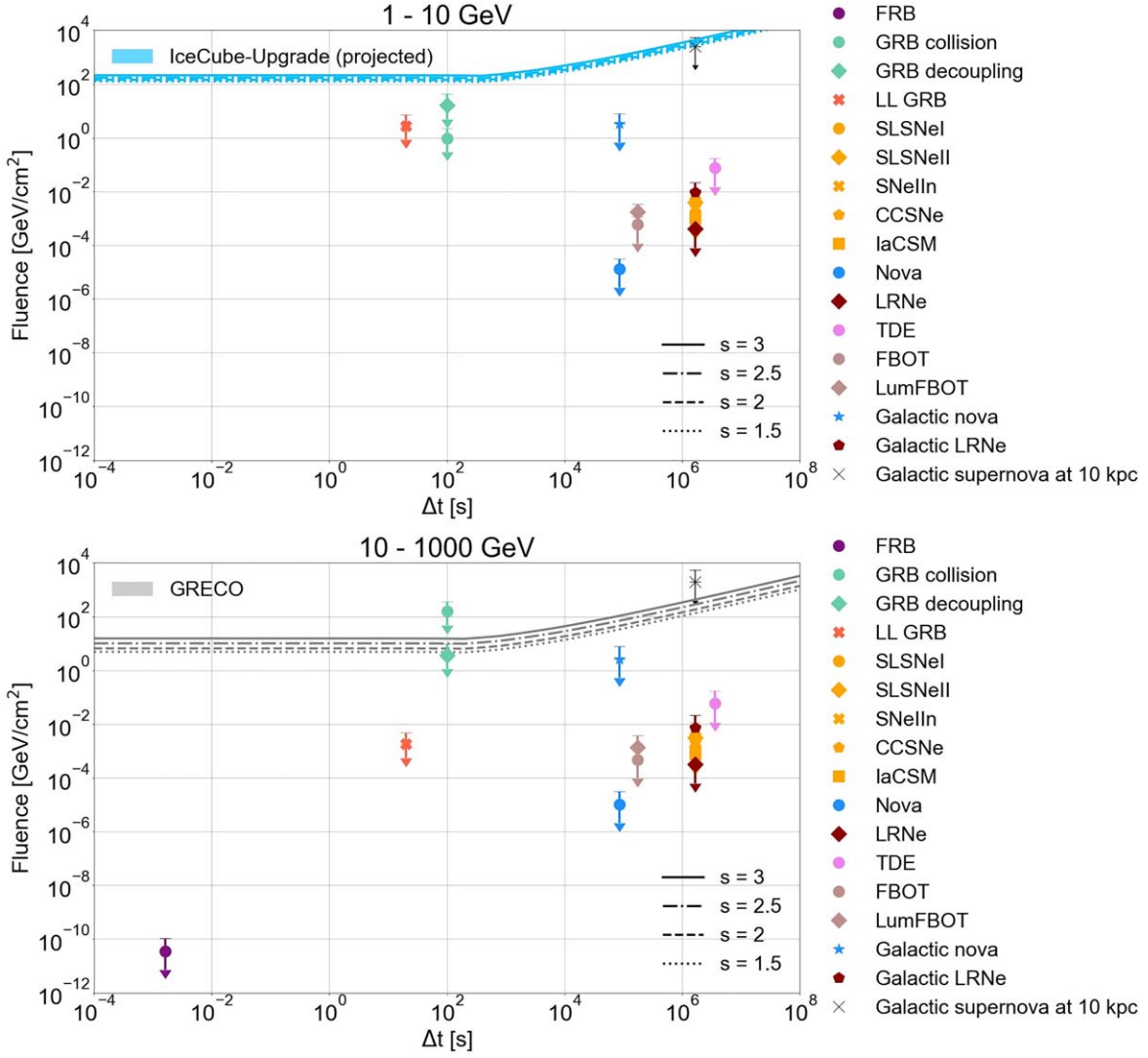


Figure 3. Predicted source fluences (time-integrated energy flux) and IceCube sensitivities integrated over 1–10 GeV (above) and 10–1000 GeV (below). The downward arrows indicate error bars with a lower value going to zero. The nearest distance of each transient type is estimated assuming 10 yr of IceCube observations. We show the estimate of FRB emission only for 10–1000 GeV, as the FRB neutrino emission is negligible at lower energies. While we also show an estimate for the fluence of a Galactic CCSN occurring at a distance of 10 kpc, this does not reflect the true rate of Galactic SNe, and it is unlikely that such a nearby event will occur in the next decade.

of interest, to show an appropriate comparison between the two quantities.

The uncertainty in the final fluence value is evaluated from the uncertainty in the observational parameters x_i , according to

$$(\Delta F_i)^2 = \sum_j \left(\frac{\partial F_i}{\partial x_j} \Delta x_j \right)^2,$$

as indicated by the error bars in Figure 3. The parameters used to evaluate the uncertainty for each transient type are:

1. *Shock-powered transients*—peak luminosity L_{pk} , mean velocity of ejecta \bar{v}_{ej} , rate R_0 , particle acceleration efficiency ϵ_{rel} , and spectral index α .
2. *Gamma-ray bursts*—isotropic-equivalent gamma-ray energy $\mathcal{E}_{\gamma, \text{iso}}$, bulk Lorentz factor Γ , nucleon loading factor ξ_N , and rate R_0 .
3. *FRBs*—radio energy \mathcal{E}_{rad} and duration t_{FRB} .

The ranges of parameters used in evaluating the error bars are intended to encompass the span of observational values for

each transient type. We take the uncertainty of each variable to be half the width of its range.

Since the aim of the predictions in Figure 3 is to demonstrate the range of signal that could be expected from a nearby transient rather than to predict the average of a population, the calculation does not consider the distribution of source luminosity. The uncertainty calculation assumes that luminosity (or isotropic-equivalent energy) and rate are independent parameters, though they could be coupled through a luminosity function. For certain source classes—such as novae, SNe, and GRBs—a luminosity function will not significantly alter the results. The luminosity functions of novae and SNe generally follow a normal distribution (W. Li et al. 2011; A. W. Shafter 2017; K. De et al. 2021), though they vary with subclass and host galaxy type. The distributions of $\mathcal{E}_{\gamma, \text{iso}}$ for HLGRBs and LLGRBs are relatively flat within the range considered in Table 1 (A. Pescalli et al. 2015; J.-L. Atteia et al. 2017). In contrast, both LRNe and TDEs exhibit steep luminosity functions, $dN/dL \propto L^{-2.5}$ (S. van Velzen 2018;

V. R. Karambelkar et al. 2023), suggesting that the neutrino fluence of a future event will likely be closer to the lower end of our estimates. Finally, in the case of Galactic FRBs, both the rate and luminosity function remain largely unknown, so the effects of considering a luminosity function cannot be determined with confidence.

5. Discussion

The predicted fluence of all shock-powered transients falls far below the sensitivity of the IceCube Upgrade and DeepCore, indicating that sources of this nature are unlikely to be detected by future observations, unless the source rates are much higher than expected. Similarly, while a Galactic FRB may have significant neutrino emission at >1 TeV, the FRB emission in giga-electronvolt neutrinos falls far below the DeepCore and Upgrade sensitivities. It is worth noting that the FRB estimate used in this work is already very optimistic, as it uses observational parameters consistent with the extragalactic FRB population, but is based on the distance of the nearby Galactic FRB 200428. In particular, while this event was similar to the extragalactic FRB population, it still had significantly lower energy than its extragalactic counterparts.

Notably, our analysis suggests that even Galactic novae are unlikely to be detected within the next decade. In particular, the nearby nova T Coronae Borealis (B. E. Schaefer 2009, 2023), which is predicted to occur in the near future and has been anticipated to be a bright neutrino source, is not likely to easily be observed using IceCube-DeepCore. This said, a recurrent nova may require consideration of different neutrino spectra and light curves than those used in our model, and a more precise analysis could yield more favorable results. Similarly, while the prospects of observing a nearby Galactic SN could be favorable, with a rate of ~ 3.2 per century, such an event has only about a 30% chance of occurring in the next decade.

To date, no GRB has been detected by IceCube, despite dedicated GRECO searches, most notably a search for the “brightest of all time” GRB 221009A (R. Abbasi et al. 2023b, 2024b). The discrepancy between models predicting GRB detections suggests that the current nondetection of any GRB may be due to large uncertainties in the composition of the GRB jet. In particular, while it is often assumed that GRB jets contain a substantial population of free neutrons, this assumption is likely too optimistic. If continued observations and dedicated GRB searches yield further nondetection, this would be a strong indication that the current models used to describe GRBs are not consistent with observations, and GRBs may not harbor the conditions necessary for substantial neutrino production to occur.



We note that the fluence predictions and sensitivity estimates used in this work are intended to be as broad as possible, but should not be considered to be precise. In particular, the estimates of the IceCube Upgrade and DeepCore sensitivities are based on a range of spectral shapes following a power law. While this is an acceptable approximation for very short timescales, it is still not a perfect comparison to the true spectral shape of a unique transient source. Future searches, especially dedicated searches for Galactic novae or HLGRBs, could improve upon this work, by tailoring the spectral shape to the shape of the particular transient in question. In addition, after the IceCube Upgrade strings are installed, a new data sample using the full upgraded infill array (the original DeepCore plus new Upgrade strings) can be developed,

potentially providing enhanced sensitivity over this energy range.

Acknowledgments

The work of A.P. and K.F. is supported by the Office of the Vice Chancellor for Research and Graduate Education at the University of Wisconsin-Madison, with funding from the Wisconsin Alumni Research Foundation. K.F. acknowledges support from the National Science Foundation (PHY-2110821 and PHY-2238916) and NASA (NMH211ZDA001N-Fermi). This work was supported by a grant from the Simons Foundation (00001470; K.F.). K.F. acknowledges the support of the Sloan Research Fellowship. B.D.M. was supported in part by the NASA Fermi Guest Investigator Program, through grant 80NSSC24K0408, and through the NASA ATP Program, through grant 80NSSC22K080. The Flatiron Institute is supported by the Simons Foundation. The work of J.V. and J.T. is supported in part by Vilas Associate funding from the Office of the Vice Chancellor for Research and Graduate Education at the University of Wisconsin-Madison and the National Science Foundation (PHY-1913607).

ORCID iDs

Angelina Partenheimer  <https://orcid.org/0009-0007-2369-258X>
 Jessie Thwaites  <https://orcid.org/0000-0001-9179-3760>
 K. Fang  <https://orcid.org/0000-0002-5387-8138>
 Justin Vandenbroucke  <https://orcid.org/0000-0002-9867-6548>
 Brian D. Metzger  <https://orcid.org/0000-0002-4670-7509>

References

- Aartsen, M. G., Abraham, K., Ackermann, M., et al. 2016, *ApJ*, 816, 75
 Aartsen, M. G., Ackermann, M., Adams, J., et al. 2019, *BAAS*, 51, 288
 Abbasi, R., Ackermann, M., Adams, J., et al. 2022, *JCAP*, 2022, 027
 Abbasi, R., Ackermann, M., Adams, J., et al. 2023a, *ApJ*, 953, 160
 Abbasi, R., Ackermann, M., Adams, J., et al. 2023b, *ApJL*, 946, L26
 Abbasi, R., Ackermann, M., Adams, J., et al. 2023c, *ApJ*, 959, 96
 Abbasi, R., Ackermann, M., Adams, J., et al. 2024a, *ApJ*, 971, 191
 Abbasi, R., Ackermann, M., Adams, J., et al. 2024b, *ApJ*, 964, 126
 Acciari, V. A., Ansoldi, S., Antonelli, L. A., et al. 2022, *NatAs*, 6, 689
 Ackermann, M., Ajello, M., Albert, A., et al. 2014, *Sci*, 345, 554
 Ackermann, M., Arcavi, I., Baldini, L., et al. 2015, *ApJ*, 807, 169
 Adams, S. M., Kochanek, C. S., Beacom, J. F., Vagins, M. R., & Stanek, K. Z. 2013, *ApJ*, 778, 164
 Aharonian, F., Ait Benkhali, F., Angüner, E. O., et al. 2022, *Sci*, 376, 77
 Andreoni, I., Coughlin, M. W., Criswell, A. W., et al. 2024, *Aph*, 155, 102904
 Andrews, J. E., & Smith, N. 2018, *MNRAS*, 477, 74
 Arcavi, I., Gal-Yam, A., Sullivan, M., et al. 2014, *ApJ*, 793, 38
 Arnett, W. D. 1982, *ApJ*, 253, 785
 Atteia, J.-L., Heussaff, V., Dezalay, J.-P., et al. 2017, *ApJ*, 837, 119
 Aydi, E., Sokolovsky, K. V., Chomiuk, L., et al. 2020, *NatAs*, 4, 776
 Bahcall, J. N., & Mészáros, P. 2000, *PhRvL*, 85, 136 2
 Bartos, I., Beloborodov, A. M., Hurley, K., & Márka, S. 2013, *PhRvL*, 110, 241101
 Beloborodov, A. M. 2010, *MNRAS*, 407, 1033
 Beloborodov, A. M. 2017, *ApJL*, 843, L26
 Bochenek, C. D., Dwarkadas, V. V., Silverman, J. M., et al. 2017, *MNRAS*, 473, 336
 Bochenek, C. D., Ravi, V., Belov, K. V., et al. 2020, *Natur*, 587, 59
 Bykov, A., Romansky, V., & Osipov, S. 2022, *Univ*, 8, 32
 Caprioli, D., & Spitkovsky, A. 2014, *ApJ*, 783, 91
 Carpio, J. A., Ekanger, N., Bhattacharya, M., Murase, K., & Horiuchi, S. 2024, *PhRvD*, 110, 083012
 Cheung, C. C., Jean, P., Shore, S. N., et al. 2016, *ApJ*, 826, 142
 Cheung, C. C., Johnson, T. J., Jean, P., et al. 2022, *ApJ*, 935, 44
 Copejans, D. L., Margutti, R., Terreran, G., et al. 2020, *ApJL*, 895, L23

- Cristofari, P., Renaud, M., Marcowith, A., Dwarkadas, V. V., & Tatischeff, V. 2020, *MNRAS*, **494**, 2760
- Dai, L., & Fang, K. 2017, *MNRAS*, **469**, 1354
- De, K., Kasliwal, M. M., Hankins, M. J., et al. 2021, *ApJ*, **912**, 19
- Diesing, R., Metzger, B. D., Aydi, E., et al. 2023, *ApJ*, **947**, 70
- Dilday, B., Howell, D. A., Cenko, S. B., et al. 2012, *Sci*, **337**, 942
- Drout, M. R., Chornock, R., Soderberg, A. M., et al. 2014, *ApJ*, **794**, 23
- Ekanger, N., Bhattacharya, M., & Horiuchi, S. 2022, *MNRAS*, **513**, 405
- Fang, K., & Metzger, B. D. 2017, *ApJ*, **849**, 153
- Fang, K., Metzger, B. D., Murase, K., Bartos, I., & Kotera, K. 2019, *ApJ*, **878**, 34
- Fang, K., Metzger, B. D., Vurm, I., Aydi, E., & Chomiuk, L. 2020, *ApJ*, **904**, 4
- Gezari, S., Chornock, R., Rest, A., et al. 2012, *Natur*, **485**, 217
- Gottlieb, O., & Globus, N. 2021, *ApJL*, **915**, L4
- Gradshteyn, I., & Ryzhik, I. 2007, Table of Integrals, Series, and Products, 7th ed. (San Diego, CA: Elsevier Academic Press)
- Guépin, C., Kotera, K., Barausse, E., Fang, K., & Murase, K. 2018, *A&A*, **616**, A179
- Gupta, N., & Zhang, B. 2007, *Aph*, **27**, 386
- Hachisu, I., & Kato, M. 2018, *ApJS*, **237**, 4
- Hambleton, K. M., Bianco, F. B., Street, R., et al. 2023, *PASP*, **135**, 105002
- Honda, M., Athar, M. S., Kajita, T., Kasahara, K., & Midorikawa, S. 2015, *PhRvD*, **92**, 023004
- Howitt, G., Stevenson, S., Vigna-Gómez, A., et al. 2020, *MNRAS*, **492**, 3229
- IceCube Collaboration 2020, Icecube Upgrade Neutrino Monte Carlo Simulation doi:10.21234/qfz1-yh02
- Insera, C. 2019, *NatAs*, **3**, 697
- Ishihara, A. 2019, *ICRC (Madison, WI)*, **36**, 1031
- Jiang, Y.-F., Guillochon, J., & Loeb, A. 2016, *ApJ*, **830**, 125
- Kachelrieß, M., Moskalenko, I., & Ostapchenko, S. 2019, *CoPhC*, **245**, 106846
- Kalaczyński, P. 2021, in 40th International Conference on High Energy physics (ICHEP2020) (Trieste: SISSA), **149**
- Kamae, T., Karlsson, N., Mizuno, T., Abe, T., & Koi, N. 2006, *ApJ*, **647**, 692
- Karambelkar, V. R., Kasliwal, M. M., Blagorodnova, N., et al. 2023, *ApJ*, **948**, 137
- Kashyap, V. L., van Dyk, D. A., Connors, A., et al. 2010, *ApJ*, **719**, 900
- Kimura, S. S., Murase, K., Mészáros, P., & Kiuchi, K. 2017, *ApJL*, **848**, L4
- Kochanek, C. S. 2014, *ApJ*, **785**, 28
- Koldobskiy, S., Kachelrieß, M., Lskavyan, A., et al. 2021, *PhRvD*, **104**, 123027
- Levinson, A., & Nakar, E. 2020, *PhR*, **866**, 1
- Li, K.-L., Metzger, B. D., Chomiuk, L., et al. 2017, *NatAs*, **1**, 697
- Li, W., Chornock, R., Leaman, J., et al. 2011, *MNRAS*, **412**, 1473
- Li, W., Leaman, J., Chornock, R., et al. 2011, *MNRAS*, **412**, 1441
- Lorimer, D. R., Bailes, M., McLaughlin, M. A., Narkevic, D. J., & Crawford, F. 2007, *Sci*, **318**, 777
- Margalit, B., Beniamini, P., Sridhar, N., & Metzger, B. D. 2020, *ApJL*, **899**, L27
- Margutti, R., Metzger, B. D., Chornock, R., et al. 2019, *ApJ*, **872**, 18
- Mason, P., & Dubus, G. 2013, *A&A*, **551**, A37
- Mason, E., Diaz, M., Williams, R. E., Preston, G., & Bensby, T. 2010, *A&A*, **516**, A108
- Matsumoto, T., & Metzger, B. D. 2022, *ApJ*, **938**, 5
- Mészáros, P. 2006, *RPPh*, **69**, 2259
- Metzger, B. D., Fang, K., & Margalit, B. 2020, *ApJL*, **902**, L22
- Metzger, B. D., Finzell, T., Vurm, I., et al. 2015, *MNRAS*, **450**, 2739
- Metzger, B. D., Giannios, D., & Horiuchi, S. 2011, *MNRAS*, **415**, 2495
- Metzger, B. D., Margalit, B., & Sironi, L. 2019, *MNRAS*, **485**, 4091
- Metzger, B. D., & Pejcha, O. 2017, *MNRAS*, **471**, 3200
- Mockler, B., Guillochon, J., & Ramirez-Ruiz, E. 2019, *ApJ*, **872**, 151
- Moriya, T. J., Sorokina, E. I., & Chevalier, R. A. 2018, *SSRv*, **214**, 59
- Murase, K., Franckowiak, A., Maeda, K., Margutti, R., & Beacom, J. F. 2019, *ApJ*, **874**, 80
- Murase, K., Ioka, K., Nagataki, S., & Nakamura, T. 2006, *ApJL*, **651**, L5
- Murase, K., Kashiyama, K., & Mészáros, P. 2013, *PhRvL*, **111**, 131102
- Murase, K., Kimura, S. S., Zhang, B. T., Oikonomou, F., & Petropoulou, M. 2020, *ApJ*, **902**, 108
- Murase, K., Mukhopadhyay, M., Kheirandish, A., Kimura, S. S., & Fang, K. 2022, *ApJL*, **941**, L10
- Nakar, E. 2015, *ApJ*, **807**, 172
- Perley, D. A., Mazzali, P. A., Yan, L., et al. 2018, *MNRAS*, **484**, 1031
- Pescalli, A., Ghirlanda, G., Salafia, O. S., et al. 2015, *MNRAS*, **447**, 1911
- Piran, T. 2005, *RvMP*, **76**, 1143
- Piran, T., Svirski, G., Krolik, J., Cheng, R. M., & Shiokawa, H. 2015, *ApJ*, **806**, 164
- Prentice, S. J., Maguire, K., Smartt, S. J., et al. 2018, *ApJL*, **865**, L3
- Quimby, R. M., Yuan, F., Akerlof, C., & Wheeler, J. C. 2013, *MNRAS*, **431**, 912
- Renault-Tinacci, N., Kotera, K., Neronov, A., & Ando, S. 2018, *A&A*, **611**, A45
- Roth, N., Kasen, D., Guillochon, J., & Ramirez-Ruiz, E. 2016, *ApJ*, **827**, 3
- Schaefer, B. E. 2009, *ApJ*, **697**, 721
- Schaefer, B. E. 2023, *MNRAS*, **524**, 3146
- Shafter, A. W. 2017, *ApJ*, **834**, 196
- Sironi, L., & Spitkovsky, A. 2010, *ApJ*, **726**, 75
- Steinberg, E., & Metzger, B. D. 2018, *MNRAS*, **479**, 687
- Stone, N. C., & Metzger, B. D. 2015, *MNRAS*, **455**, 859
- Taylor, M., Cinabro, D., Dilday, B., et al. 2014, *ApJ*, **792**, 135
- The Fermi-LAT Collaboration 2014, *Sci*, **345**, 554
- The Fermi-LAT Collaboration, Abdo, A. A., Ackermann, M., et al. 2010, *Sci*, **329**, 817
- Tylenda, R., Hajduk, M., Kamiński, T., et al. 2011, *A&A*, **528**, A114
- van Velzen, S. 2018, *ApJ*, **852**, 72
- van Velzen, S., Holoien, T. W.-S., Onori, F., Hung, T., & Arcavi, I. 2020, *SSRv*, **216**, 124
- Velzen, S. v. 2018, *ApJ*, **852**, 72
- Virgili, F. J., Liang, E.-W., & Zhang, B. 2009, *MNRAS*, **392**, 91
- Wanderman, D., & Piran, T. 2010, *MNRAS*, **406**, 1944
- Winter, W., & Lunardini, C. 2023, *ApJ*, **948**, 42
- Xu, R., Spitkovsky, A., & Caprioli, D. 2020, *ApJL*, **897**, L41
- Zegarelli, A., Celli, S., Capone, A., et al. 2022, *PhRvD*, **105**, 083023